FLOW SIMULATION OVER THE COMPLETE VLS SYSTEM USING A CHIMERA APPROACH

Alexandre P. Antunes - alex@iae.cta.br
Centro Técnico Aeroespacial, Instituto Tecnológico de Aeronáutica
CTA/ITA/IEAA – 12228-900 –São José dos Campos, SP, Brazil.
Edson Basso - basso@iae.cta.br
Centro Técnico Aeroespacial, Instituto Tecnológico de Aeronáutica
CTA/ITA/IEAA – 12228-900 –São José dos Campos, SP, Brazil.
João Luiz F. Azevedo - azevedo@iae.cta.br
Centro Técnico Aeroespacial, Instituto de Aeronáutica e Espaço
CTA/IAE/ASE-N – 12228-904 –São José dos Campos, SP, Brazil.

Abstract. *The present work is part of the effort for the development of computational tools necessary to simulate aerodynamic flows over aerospace geometries, especially those related to the first Brazilian Satellite Launch Vehicle, VLS. Aerodynamic flow simulations over the VLS during its first-stage flight are presented together with a validation effort of these results through the use of wind tunnel experimental data available for the vehicle. The calculations use the Chimera technique together with block structured grids to discretize the computational domain. The current approach is based on the solution of the 3-D Euler equations in curvilinear coordinates. A finite difference method is applied to these equations and a centered spatial discretization is used. Artificial dissipation terms, based on a scalar, non-isotropic model, are added. The time march process is accomplished with a 5-stage, 2nd-order accurate, Runge-Kutta scheme.*

Keywords: *Multiblock technique, Chimera, VLS, Finite differences.*

1. INTRODUCTION

In the present work, the overset multiblock grid technique, or Chimera (Wang and Yang,1994, Wang, Buning, and Benek, 1995), is used to simulate flows over the complete first Brazilian Satellite Launcher, VLS. The VLS presents a quite complex geometric configuration during its first-stage flight, because it is composed of four strap-on booster arranged symmetrically around a central core. Therefore, mesh generation for flow simulation during the

first-stage flight can be a very laborious process either with structured or unstructured grid technologies. The initial attempts to generate a good structured grid over the complete VLS configuration resorted to a patched multiblock approach. However, the quality of the meshes generated was not adequate for the flow simulations intended and, therefore, the use of patched grids was discarded. The desired quality for the meshes was achieved by the use of overset multiblock meshes, or Chimera grids. This technique provides the capability to use structured meshes for the discretization of the calculation domain over truly complex configurations. Moreover, it allows grid refinement characteristic which are almost similar to those achieved with unstructured meshes.

The code for the simulation of the flow over the VLS with this overset multiblock approach was obtained as a continuation of the development of the code already available for single-block flow simulations (Bigarelli, Mello and Azevedo,1999). The governing equations are assumed to be written in conservative form. These equations are discretized in a finite difference context. Spatial discretization uses second-order accurate, central difference operators. The time march method is based on a 5-stage, Runge-Kutta algorithm (Jameson, Schmidt and Turkel,1981), which also has second-order accuracy in time. The artificial dissipation terms added are based on the non-isotropic, Turkel and Vatsa (1994) model. The paper is inserted into the effort of developing the computational tools necessary to simulate aerodynamic flows on aerospace configurations (Azevedo, Menezes and Fico, 1995, PartI and II, Azevedo, Strauss and Ferrari,1997, and Strauss and Azevedo,1999). It briefly describes the theoretical formulation used together with a discussion of the numerical implementation aspects and boundary conditions adopted. Results that demonstrate the capability implemented are presented and discussed.

2. THEORETICAL FORMULATION

It is assumed that the flows of interest in the present work can be represented by the Euler equations in three dimensions. These equations can be written in conservation-law form for a curvilinear coordinate system as

$$\frac{\partial \overline{Q}}{\partial \tau} + \frac{\partial \overline{E}}{\partial \xi} + \frac{\partial \overline{F}}{\partial \eta} + \frac{\partial \overline{G}}{\partial \varsigma} = 0 \quad , \tag{1}$$

where $\overline{Q}$ is the vector of conserved variables, defined as

$$\overline{Q} = J^{-1}\left[\rho, \rho u, \rho v, \rho w, e\right]^T \quad . \tag{2}$$

In these equations, ρ is the density, *u*, *v*, *w* are the Cartesian velocity components and *e* is the total energy per unit of volume. The $\overline{E}, \overline{F}$ and $\overline{G}$ are the inviscid flux vectors, *J* is the Jacobian of the transformation, represented as

$$J = \left(x_\xi\, y_\eta\, z_\varsigma + x_\eta\, y_\varsigma\, z_\xi + x_\varsigma\, y_\xi\, z_\eta - x_\xi\, y_\varsigma\, z_\eta - x_\eta\, y_\xi\, z_\eta - x_\varsigma\, y_\eta\, z_\xi\right)^{-1} \quad . \tag{3}$$

Expressions for the inviscid flux vector can be found in Azevedo and Buonomo (1999), among other references. The pressure can be obtained from the equation of state for a perfect gas as

$$p=(\gamma-1)\left[\, e-\frac{1}{2}\rho\left(u^2+v^2+w^2\right)\right] \quad . \tag{4}$$

A suitable nondimensionalization (Pulliam and Steger, 1980) of the governing equations has been assumed in order to write Eq. (1). In particular, the values of flow properties are made dimensionless with respect to freestream quantities, as described in Pulliam and Steger (1980).

The governing equations are discretized by a finite difference scheme on structured hexahedral meshes which would conform to the bodies in the computational domain. Since a central difference spatial discretization method is being used, artificial dissipation terms must be added to the formulation in order to control nonlinear instabilities. The artificial dissipation terms used here are based on Turkel and Vatsa's (1994) scalar model. This model is nonlinear and non-isotropic, with the scaling of the artificial dissipation operator in each coordinate direction weighted by its own spectral radius of the corresponding flux Jacobian matrix. In the present implementation, the residue operator is defined as

$$RHS^n = -\Delta t\left(\delta_\xi E^n + \delta_\eta F^n + \delta_\varsigma G^n\right) \quad . \tag{5}$$

Here, the δ_ξ , δ_η and δ_τ terms represent mid-point central difference operators in the ξ, η and ς directions, respectively. The numerical flux vectors are defined as

$$\begin{aligned}
E_{i\pm\frac{1}{2},j,k} &= \frac{1}{2}\left(E_{i,j,k} + E_{i+1,j,k}\right) - d_{i\pm\frac{1}{2},j,k} \quad , \\
F_{i,j\pm\frac{1}{2},k} &= \frac{1}{2}\left(F_{i,j,k} + F_{i,j+1,k}\right) - d_{i,j\pm\frac{1}{2},k} \quad , \\
G_{i,j,k\pm\frac{1}{2}} &= \frac{1}{2}\left(G_{i,j,k} + G_{i,j,k+1}\right) - d_{i,j,k\pm\frac{1}{2}} \quad .
\end{aligned} \tag{6}$$

The artificial dissipations operators, $d_{i\pm\frac{1}{2},j,k}$, $d_{i,j\pm\frac{1}{2},k}$ and $d_{i,j,k\pm\frac{1}{2}}$, are defined precisely as described in Turkel and Vatsa's (1994) model.

Since steady state solutions are the major interest of the present study, a variable time step convergence acceleration procedure has been implemented. In the present case, the time step is defined as

$$\Delta t_{i,j,k} = \frac{CFL}{c_{i,j,k}} \quad . \tag{7}$$

The characteristic velocity , $c_{i,j,k}$, is defined as

$$c_{i,j,k} = \max\left(\left|U\right| + a\sqrt{\xi_x^2+\xi_y^2+\xi_z^2}\ ,\ \left|V\right| + a\sqrt{\eta_x^2+\eta_y^2+\eta_z^2}\ ,\ \left|W\right| + a\sqrt{\varsigma_x^2+\varsigma_y^2+\varsigma_z^2}\ \right)_{i,j,k}, \tag{8}$$

where *a* is the speed of sound and *U*, *V*, and *W* are the contravariant velocity components.

The time march is performed based on a 5-stage, 2nd-order accurate, hybrid Runge-Kutta time-stepping scheme, where

$$
\begin{aligned}
&Q_i^{(0)} = Q_i^n \\
&Q_i^{(l)} = Q_i^{(0)} - \alpha_l \, RHS^{(l-1)} \quad , l = [1..5] \, , \\
&Q_i^{n+1} = Q_i^{(5)} \quad ,
\end{aligned} \tag{9}
$$

where $\alpha_1 = \frac{1}{4}$, $\alpha_2 = \frac{1}{6}$, $\alpha_3 = \frac{3}{8}$, $\alpha_4 = \frac{1}{2}$, $\alpha_5 = 1$. It should be emphasized that only the convective operator inside the RHS term indicated in Eq. (9) is actually evaluated at every time step. The artificial dissipation terms are only evaluated in the first and second stages of the time-march procedure. It can be shown that this provides enough damping to maintain nonlinear stability (Jameson, Schmidt and Turkel,1981), whereas it yields a more efficient numerical scheme.

3. BOUNDARY CONDITIONS

The boundary conditions for the rocket surface are based on the fact that there should be no flow through a solid surface. This is imposed in the present context by forcing the contravariant velocity component normal to the wall, V, to be identically zero in the flux calculations. Aside from this boundary condition enforcement at the flux calculation stage, conserved properties at the wall points are simply obtained by zero-th order extrapolation of their nearest neighbors in the nominally wall-normal direction. Although extremely simple, this boundary condition enforcement procedure has proved to be quite adequate with the present algorithm (Vieira *et.al.*,1998).

Freestream conditions are imposed at the upstream and lateral far-field boundaries. Symmetry boundary conditions are used at the upstream centerline, and all quantities are obtained by extrapolation of interior data at the downstream boundaries. Zero-th order extrapolation is used in this latter case, in order to simplify the code implementation. Interior boundaries which are created by the multiblock approach are handled by the Chimera property interpolation procedure which is described in the next section.

4. CHIMERA TECHNIQUE

The mesh point distribution over the physical domain in which the flow is to be computed is always a critical aspect for a successful calculation. Grid point distribution must be balanced so as to cover the entire flowfield, avoiding regions with excessive grid coarseness. On the other hand, points must be clustered in regions in which phenomena, such as expansions and shock waves, occur without exceeding the available computational resources. The computational meshes used in the present work are all generated by the multisurface algebraic technique described by Fletcher (1988). For the VLS configuration, five component meshes are generated, one for each body which forms the complete configuration. Figure 1 exhibits the surface mesh for the complete VLS configuration.

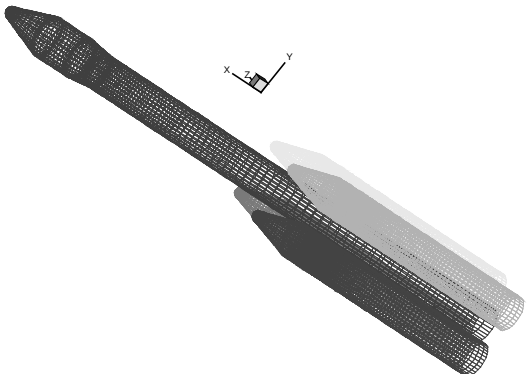

Figure 1. Detail of the surface body meshes for the complete VLS configuration

Although the present work is concerned with Euler solutions, the meshes contain a large number of points near the wall as a attempt to capture details of the shock reflection phenomena which are expected to occur in the cluster region. Another important aspect is the need for a sufficient number of points between the lateral boosters and the central rocket for an adequate behavior of the Chimera hole-cutting process. In this process, points of both meshes are eliminated from the set of active points in the domain either for being outside the flow regions of interest or in order to avoid an excessively large region of overlap. Larger regions of overlap can improve the accuracy of information exchange at the expense of increasing the computational costs. The present work uses trilinear interpolation in order to pass information to the interior boundary points of each mesh. There is no attempt to satisfy conservation in this interpolation

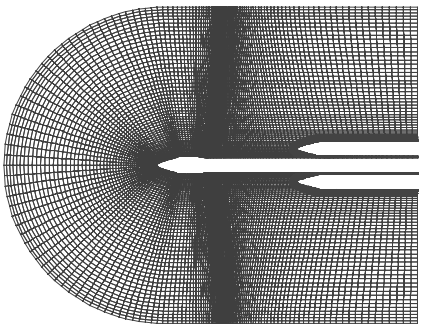

Figure 2 – Configuration after the hole-cutting process, 2-D visualization for the complete VLS configuration

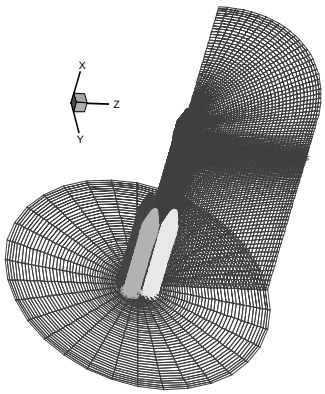

Figure 3. Three-dimensional view of the VLS mesh.

process due to the high computational cost associate with such an implementation in the 3-D case. A conservative method at the interfaces among Chimera meshes that satisfies the conservation law was developed by Wang and Yang (1994). A detailed discussion of the approaches for handling these interior boundary conditions can be seen in Wang, Buning and Beneck (1995).

In the case of the VLS meshes, the code performs the logic elimination of the mesh points that are inside the other bodies and, therefore, out of the calculation domain. Figure 2 represents one longitudinal plane of the meshes for the complete VLS configuration after the hole-cutting process. A 3-D view of the meshes is presented in Fig. 3 . Moreover, a detail of the downstream portion of the central body mesh, already indicating the hole for the boosters, is shown in Fig. 4.

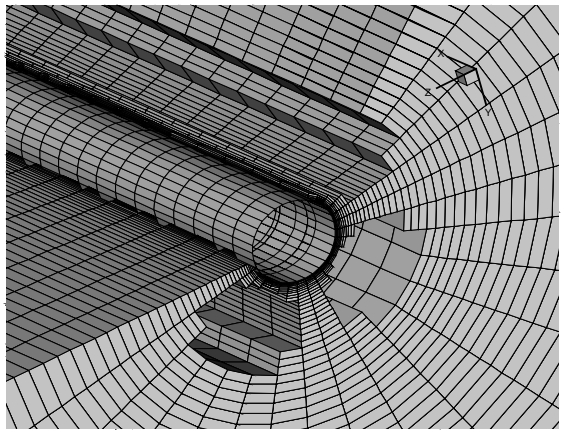

Figure 4- Detail of the meshes for the complete VLS configuration after the hole-cutting process: a 3-D visualization

The solution process in the flow solver can be essentially separated in the following steps:

1. An initial condition is imposed for all meshes;
2. An order of operation throughout the various meshes is defined;
3. The residue is calculated in the first mesh;
4. The new solution is calculated for the first mesh interior points;
5. Boundary conditions are updated for this first mesh;
6. The points along the hole boundary are updated in all meshes which overlap with this first mesh;
7. The process is restarted from step (3) with the next mesh.

This process is repeated until all the meshes have reached the new solution level at time $(n+1)\,\Delta t$. Afterwards, convergence of the solution is verified. If the convergence criterion is not satisfied, the process is restarted from step (3).

5. RESULTS AND DISCUSSION

The results here presented refer to simulations of the flow over the VLS vehicle during its first-stage flight. The specific results included consider only the case with freestream Mach number $M_\infty = 2$ and zero angle of attack, which is representative of the numerical simulations performed so far for this configuration. Moreover, as the flight time in the lower atmosphere for these satellite launchers is very short and the vehicle is at supersonic speeds during most of this flight, a supersonic flight condition is considered more representative of the vehicle operation. Moreover, within the supersonic speed regime, several interesting aspects of the multiblock mesh

technology can be analyzed, such as the communication of information across the internal boundaries among blocks with discontinuities in the flow properties.

The complete mesh system used in the present simulations was divided into five component meshes. One of these discretizes the computational domain around the central body using 120 X 65 X 33 grid points in the ξ, η, ζ directions, respectively. Four identical meshes are used for the boosters. Each of them has 120 X 36 X 33 grid points in the longitudinal, normal and circumferential directions, or ξ, η, and ζ directions, respectively. Typical grids use in the present simulations have already been shown in Figs. 1-4.

Mach number contours along the vehicle body walls can be seen in Fig. 5. The strong flow compressions in the rocket front areas can be clearly seen in this figure, indicating the flow stagnation points. One can also see in Fig. 5 a region of low speed along the central body wall, somewhat downstream of the booster noses. This region is associated with the boosters' detached front shock, which converge along the central body creating a high pressure, and low speed, region. This high pressure region causes the flow streamlines to deviate from the boosters, yielding some relief in the pressure at the boosters' noses and, therefore, causing smaller pressure levels at the booster's fairing than those observed in the main fairing.

Figure 6 exhibits Mach number contours along the surface of the central body and two of the boosters. One should observe that the booster that would be in front of the central body, considering a lateral view, has been removed in order to allow the visualization of the contours along the central core. The several regions affected by the detached shocks on the boosters can be seen in Fig.6. Moreover, one can also clearly see that the solution along the two boosters is symmetric, as one should expect for this zero angle of attack case. It would be very interesting to include enlarged views of the flow regions with stronger interactions. However, due to paper size constraints, this has not been done here.

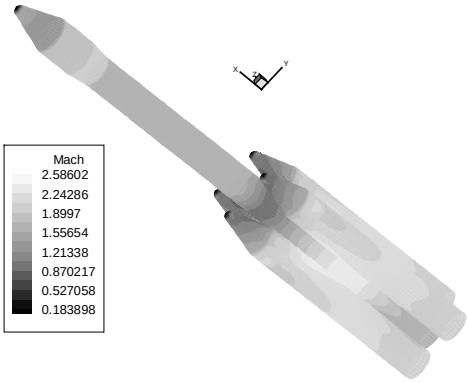

Figure 5. Mach number contours on the surface of the vehicle for $M_\infty = 2.0$ and zero angle of attack

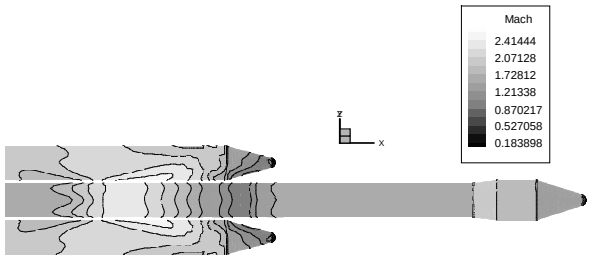

Figure 6: Mach number contours on the central body and two opposing booster for the VLS at $M_\infty = 2.0$ and $\alpha = 0$ deg.

In Fig.7, a longitudinal flow plane which contains the central body and two boosters is presented. This figure clearly indicates the bow shock wave ahead of the vehicle, the expansion which occurs at the forebody cone-cylinder intersection, the expansion region along the boattail, and the compression region ahead of the boosters. One should also observe that a shock is formed at the downstream portion of the boattail, due to the existence of a recompression corner. This

can also be clearly seen in the Fig. 7. The complexity of the flow in the region of the boosters can also be appreciated in Fig.7. It should be noted, however, that the grid resolution is not yet adequate to capture the shock reflections between the central body and the boosters. One of the reasons for the selection of the present test case was the existence of experimental data for this flight condition. This experimental data and details of the wind tunnel tests are described in Moraes and Neto (1990). Figure 8 exhibits a comparison of the calculated pressure coefficient, *Cp*, distributions along the vehicle's central body with the experimental data. In this case, a longitudinal plane which contains the central body and two booster axes was selected for the comparison. In other words, the comparison is indicating the agreement of the data for a plane of the central body corresponding to the cut indicated in Fig.7. One can observe that the agreement in the forebody portion of the vehicle is very good. The agreement in the afterbody region, especially where there is a close proximity between central body and booster, is not as good. However, some aspects of the results in this downstream portion of the vehicle can be explained and/or deserve further comment. First of all, one should observe that the experimental data does indicate the reflection of the booster bow shock wave at x/L approximately equal to 0.6. As previously discussed, the grid resolution was not fine enough to capture this phenomenon in the numerical calculations. The striking difference in the results downstream of x/L ≅ 0.92 is due to the fact that the central body nozzle was not modeled in the present calculations whereas it was present in the wind tunnel model. There is also a fair amount of difference in the *Cp* distributions in the 0.75<x/L<0.90 range. At this point, the authors are attributing these differences to the lack of resolution of the computational mesh in this region. Grid refinement studies are currently being performed in order to try to resolve these difficulties. Furthermore, comparisons similar to the one presented in Fig.8 could be performed for other longitudinal planes along the central body and also along the boosters. These have not been included in the present paper in the interest of brevity and because the results already indicated in this figure are representative of the quality of agreement which has been obtained in the simulations performed so far. It should be further observed that the present paper is reporting on a ongoing research effort in which the results obtained thus far are very encouraging. Nevertheless, the validation of the results is a process still being performed, which is essential for the actual use of the tools here presented in a realistic production environment.

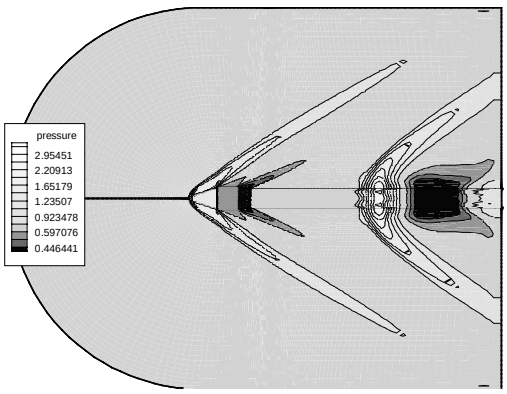

Figure 7. Pressure contours for a longitudinal plane with two boosters for $M = 2.0$ and $\alpha = 0$ deg.

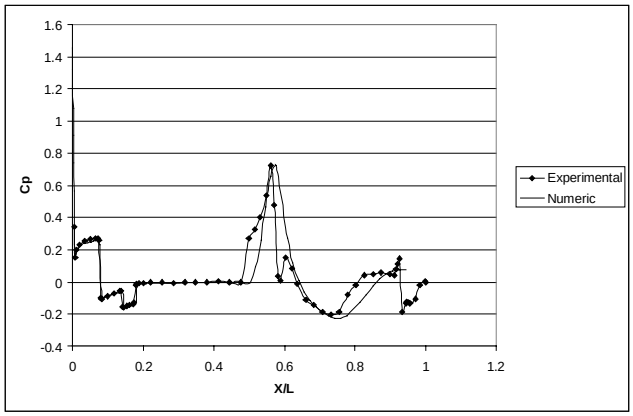

Figure 8. Comparison of central body pressure coefficient distributions for a longitudinal plane including a booster for $M = 2.0$ and $\alpha = 0$ deg.

6. CONCLUDING REMARKS

The paper has presented results for 3-D Euler simulations of the flow over the complete first-stage flight configuration of the first Brazilian Satellite Launcher, the VLS. To the authors knowledge, this is the first time that such accurate and detailed simulations of the flow over the VLS are performed and presented. A structured multiblock code has been implemented, using a Chimera approach for handling the geometric complexity of the configuration.

The procedure implemented has been applied to flow simulation at supersonic speeds for the VLS first-stage flight configuration, and results for $M_\infty = 2$ and zero degree angle of attack have been included in the present paper. The qualitative behavior of the numerical solution is very good for an Euler simulation. Quantitative agreement with experimental data is also very good in the forward portions of the vehicle, but the mesh clearly lacks refinement for a better resolution of the downstream portions of the flowfield. There was no apparent degradation of the quality of the flow solution due to the fact that there are shock waves crossing the boundary between overset meshes. A detailed account of the grid overlapping effects is beyond the scope of the present paper, but it is sufficient to state here that the overall smoothness of the numerical solutions was very good. Nevertheless, grid refinement studies are currently being performed in order to assess the quantitative differences observed in the pressure coefficient distributions in the downstream portions of the computational domain.

7. ACKNOWLEDGEMENT

The present work was partially supported by Conselho Nacional de Desenvolvimento Científico e Tecnológico, CNPq, under the Integrated Project Research Grant No. 522413/96-0. Additional support received from CNPq in terms of graduate scholarships for the first and second authors is also gratefully acknowledged. The authors are also indebted to Núcleo de Atendimento em Computação de Alto Desempenho, NACAD-COPPE/UFRJ, which has provided the computational resources used for the present simulations.

8. REFERENCES

Azevedo, J.L.F., and Buonomo, C.A., "Axisymmetric Turbulent Simulations of Launch Vehicle Forebody Flows," AIAA Paper No. 99-3528, 30th AIAA Fluid Dynamics Conference and Exhibit, Norfolk, VA, June-July 1999.

Azevedo, J.L.F., Menezes, J.C.L., and Fico, N.G.C.R., Jr., "An Assessment of Boundary Layer Properties for Transonic and Supersonic Flows over the VLS," AIAA Paper No. 95-1769-CP, Proceedings of the 13th AIAA Applied Aerodynamics Conference, Part 1, San Diego, CA, June 1995, pp. 41-51.

Azevedo, J.L.F., Menezes, J.C.L., and Fico, N.G.C.R., Jr., "Accurate Turbulent Calculations of Transonic Launch Vehicle Flows," AIAA Paper No. 96-2484-CP, Proceedings of the 14th AIAA Applied Aerodynamics Conference, Part 2, New Orleans, LA, June 1996, pp. 841-851.

Azevedo, J.L.F., Strauss, D., and Ferrari, M.A.S., "Viscous Multiblock Simulations of Axisymmetric Launch Vehicle Flows," AIAA Paper No. 97-2300-CP, Proceedings of the 15th AIAA Applied Aerodynamics Conference, Part 2, Atlanta, GA, June 1997, pp. 664-674.

Bigarelli, E.D.V., Mello, O.A.F., and Azevedo, J.L.F., "Three Dimensional Flow Simulations for Typical Launch Vehicles at Angle of Attack," Proceedings of the 15th Brazilian Congress of Mechanical Engineering, Águas de Lindóia, SP, Brazil, Nov. 1999 (Publication in CD-ROM format without page numbering).

Fletcher, C.A.J., "Computational Techniques for Fluid Dynamics", Vol. II, Springer-Verlag, New York, 1988.

Jameson, A., Schmidt, W., and Turkel, E., "Numerical Solutions of the Euler Equations by Finite Volume Methods Using Runge-Kutta Time-Stepping Schemes," AIAA Paper No. 81-1259, June 1981.

Moraes, P., Jr., and Neto, A.A., "Aerodynamic Experimental Investigation of the Brazilian Satellite Launch Vehicle (VLS)," Proceedings of the 3rd Brazilian Thermal Sciences Meeting, Vol. I, Itapema, SC, Brazil, Dec.1990, pp. 211-215.\

Pulliam, T.H., and Steger, J.L., "Implicit Finite-Difference Simulations of Three-Dimensional Compressible Flow," AIAA Journal}, Vol. 18, No. 2, Feb. 1980, pp. 159-167.

Strauss, D., and Azevedo, J.L.F., "A Numerical Study of Turbulent Afterbody Flows Including a Propulsive Jet," AIAA Paper No. 99-3190, Proceedings of the 17th AIAA Applied Aerodynamics Conference, Norfolk, VA, June-July 1999, pp. 654-664.

Turkel, E., and Vatsa, V.N., "Effect of Artificial Viscosity on Three-Dimensional Flow Solutions," AIAA Journal, Vol. 32, No. 1, Jan. 1994, pp. 39-45.

Vieira, R., Azevedo, J.L.F., Fico, N.G.C.R., Jr., and Basso, E., "Three Dimensional Flow Simulation in the Test Section of a Slotted Transonic Wind Tunnel," ICAS Paper No. 98-R.3.11, Proceedings of the 21st Congress of the International Council of the Aeronautical Sciences}, Melbourne, Australia, Sept. 1998 (Publication in CD-ROM format without page numbering).

Wang, Z.J., and Yang, H.Q., "A Unified Conservative Zonal Interface Treatment for Arbitrarily Patched and overlapped Grids," AIAA Paper No. 94-0320, 32nd AIAA Aerospace Sciences Meeting and Exhibit, Reno, NV, Jan. 1994.

Wang, Z.J., Buning, P., and Benek, J., "Critical Evaluation of Conservative and Non-Conservative Interface Treatment for Chimera Grids," AIAA Paper No. 95-0077, 33rd AIAA Aerospace Sciences Meeting and Exhibit, Reno, NV, Jan. 1995.